

QUANTIFYING INFORMATION DISCLOSURE DURING GRADIENT DESCENT USING GRADIENT UNIQUENESS

Mahmoud Abdelghafar
 Rice University
 msm15@rice.edu

Maryam Aliakbarpour
 Rice University
 maryama@rice.edu

Chris Jermaine
 Rice University
 cmj4@rice.edu

ABSTRACT

Disclosing private information via publication of a machine learning model is often a concern. Intuitively, publishing a learned model should be less risky than publishing a dataset. But how much risk is there? In this paper, we present a principled disclosure metric called *gradient uniqueness* that is derived from an upper bound on the amount of information disclosure from publishing a learned model. Gradient uniqueness provides an intuitive way to perform privacy auditing. The mathematical derivation of gradient uniqueness is general, and does not make any assumption on the model architecture, dataset type, or the strategy of an attacker. We examine a simple defense based on monitoring gradient uniqueness, and find that it achieves privacy comparable to classical methods such as DP-SGD, while being substantially better in terms of (utility) testing accuracy.

1 INTRODUCTION

Data privacy is a crucial concern in data analytics and machine learning. The most commonly-applied definition of privacy is “differential privacy” (DP) (Dwork et al., 2006; Dwork & Roth, 2014). Intuitively, for a randomized algorithm to be differentially private, it must be the case that, whenever the algorithm is run on two input datasets A and B that are similar, the output of the algorithm is likely to be the same. That is, it should not be possible to construct a set of outputs S such that the output of the algorithm on A is much more (or less) likely to be in S than the output of the algorithm on similar dataset B .

DP as a definition deals with what happens in the very worst case. It ensures that there exists no way for an attacker to choose a set of possible outputs that can distinguish between *any* two similar input datasets. One problematic implication of the pessimism is that methods to ensure DP can be extremely disruptive. In this paper, we are concerned with mini-batch stochastic gradient descent (SGD), which powers modern AI. The differentially-private version of SGD (DP-SGD) (Abadi et al., 2016) requires adding noise to gradients as well as clipping gradients (limiting their magnitude) so that no datapoint can influence a gradient too much. Unfortunately, this is a very onerous change to the algorithm. Training a large language model (LLM) like Gemini (Google, 2025) or Llama (Grattafiori et al., 2024) can easily cost millions of dollars, and few organizations who will spend such sums will accept adding noise and truncating each and every gradient, out of concern to the quality of the resulting model. As a result, the state-of-the-art differentially private LLM (Vault-Gemma, 2025) has performance on par with GPT2 (Radford et al., 2019), a full model generation before GPT3’s capabilities captured widespread public attention (Brown et al., 2020).

Because of the impracticality of DP as a privacy metric in such situations, there has been some recent interest in new definitions of privacy that do not make worst-case assumptions. For example, one may assume a prior over datasets (in the Bayesian sense (Triastcyn & Faltings, 2020)), so that the privacy definition need not be concerned with all possible inputs, only likely ones. Such definitions may allow for less onerous privacy preservation algorithms.

However, having *any* definition of privacy that requires a user to modify SGD to match that definition is a problem if the user is unwilling to accept a change to SGD. Thus, in this paper, we look at the problem in a very different way. Specifically, we ask: Given a *particular* dataset being used to power a mini-batch SGD algorithm, can we rigorously quantify the level of disclosure by the SGD

algorithm? Mini-batch SGD has some inherent, privacy-preserving characteristics, even without modifying the algorithm at all. It is a stochastic algorithm, where randomly selected per-point gradients are summed together, and depending upon the exact scenario, an attacker will typically be able to see only final model. This naturally limits disclosure. If it is determined that points are not safe, they can then be protected by auditing the result of queries to the model (in a closed-source model). For open-source models, methods such as machine unlearning (Bourtoule et al., 2021) can be used. Or, one could simply monitor information disclosure during training and drop those points with highest disclosure. Dropping a few percent of the input data may be more acceptable than changing the training algorithm by adding noise. We explore this option experimentally.

Our Contributions. We present a mathematically derived privacy score called *gradient uniqueness* or GNQ, that monotonically increases with an upper bound on the information disclosed to an attacker by mini-batch gradient descent. Thus, GNQ provides a principled, well-justified analysis of the risk of the disclosure of individual datapoints during SGD. Specific contributions are:

- The basis of GNQ in a mathematical analysis of SGD contrasts with other, heuristic privacy scores used in empirical attack-based auditing (Sec. 2). The derivation of GNQ is general, and does not make any assumption on the model architecture, dataset type, and the adversary strategy (Sec. A).
- We show empirically the ability of GNQ to explain/predict the success rate of various attacks, as well as the impact of standard, algorithmic components of the SGD algorithm (batch size, learning rate, etc.) on the vulnerability of a learned model. (Sec. 6.2)
- While the derivation of a suite of defenses based on GNQ is left to future work, we empirically test a simple, GNQ-based defense: rank datapoints within a dataset from the highest risk to the lowest risk using GNQ, and remove those at highest risk from training. We provide a compute/memory-efficient implementation suitable for large models and datasets (Sec. 5). Our experiments consider CNN-based models like the ResNet-family and Transformer-based models like the BERT-family. We find that a GNQ-based defense achieves comparable privacy level as DP-SGD; nearly perfect protection from a membership inference attack (MIA), while being substantially better in terms of model utility. It also protects against reconstruction attacks with high model accuracy (Sec. 6.1).

2 RELATED WORK

Empirical Attack-based Privacy Auditing. Most auditing approaches probe a trained model with explicit attacks, then interpret attack success as evidence of privacy risk (Murakonda & Shokri, 2020; Nicolae et al., 2018; Trail of Bits, 2021; Kazmi et al., 2024). Common attack types and their decision statistics (a.k.a privacy scores) include: (i) shadow-model MIA (Shokri et al., 2017), which feeds the model’s posterior/confidence vector (often top- k probabilities) to an attack classifier; the per-example score is the attack model’s membership probability; (ii) white-box MIAs (Nasr et al., 2019), which use gradients, activations, and per-layer norms as features; the score is a classifier over these white-box features; (iii) loss-based MIAs (Sablayrolles et al., 2019; Watson et al., 2022), which take the (negative log-)loss on the candidate point as the score (lower loss \Rightarrow more likely member); (iv) influence-function MIAs (Cohen & Giryes, 2024), which use self-influence magnitude as the score; (v) LiRA (Carlini et al., 2022), which computes a per-example log-likelihood ratio between member and non-member *loss* distributions estimated via shadow models; (vi) model inversion (ModInv) and gradient inversion (GradInv) (Fredrikson et al., 2015; Zhu et al., 2019; Geiping et al., 2020), which do not output a membership score but optimize a reconstruction objective and evaluate privacy via reconstruction quality; and (vii) property inference (Ateniese et al., 2015; Ganju et al., 2018), which trains a meta-classifier on model outputs. Comprehensive evaluations show that attack outcomes depend on datasets, architectures, and attack strategy (Song & Mittal, 2021). Our framework does not instantiate any attack; instead, GNQ quantifies the *intrinsic* privacy risks of the training algorithm itself, yielding a theoretically-grounded, attack-agnostic auditing.

Theoretical Attack-based Privacy Auditing. Although, some efforts exist to make attack-based auditing provide some theoretical guarantees, often these efforts are limited to specific model architectures. For instance, (Murakonda et al., 2021; Ye et al., 2022) provide theoretical analyses of MIA and rely on specific models like Bayesian networks. Similarly, Wang et al. (2023) examines GradInv restricting its scope to fully connected layers. The derivation of GNQ is general, and does not make any assumption on the model architecture.

Auditing Differential Privacy. Differential privacy formalizes (ε, δ) -style guarantees for randomized algorithms (Dwork et al., 2006; Dwork & Roth, 2014). In deep learning, these guarantees are commonly obtained with DP-SGD (Abadi et al., 2016). Recent auditing methods empirically check whether implementations achieve their claimed privacy levels (Jagielski et al., 2020; Steinke et al., 2023; Nasr et al., 2023). Program-logical frameworks verify DP guarantees via proof systems (Barthe et al., 2012; Zhang & Kifer, 2017); software such as OpenDP operationalize DP mechanisms (OpenDP, 2025). By contrast, GNQ quantifies the privacy risks of trained models regardless of whether DP was used, rather than proving DP guarantees for specific randomized mechanisms.

Machine Unlearning. Machine unlearning studies removing a point’s influence and verifying deletion (Bourtoule et al., 2021; Sommer et al., 2022; Warnecke et al., 2023). GNQ is a per-iteration, per-example risk score that encapsulates how the algorithmic components of the training algorithm shape each datapoint’s risk. Hence, it can guide risk-aware, training-time unlearning and serves as a built-in metric to audit the resulting change in risk.

3 GRADIENT UNIQUENESS

In this Section, we present the central result of the paper: that “gradient uniqueness” (or GNQ)—which we define subsequently—can be used to determine the level of disclosure associated with any datapoint during execution of a mini-batch gradient descent algorithm, regardless of the model. To justify the use of GNQ, in the Appendix of the paper we argue mathematically that the amount of information available to *any* attacker, regardless of the attack strategy, in the disclosure of a model learned is bounded by a function that monotonically increases with GNQ. Thus, any defense that reduces the maximum GNQ tends to reduce the success of any attack.

Assume a public dataset $\mathcal{D} = \{d_j\}_{j=1}^N$ from which the private dataset \mathcal{D}_t is sampled uniformly at random without replacement. The sampling distribution serves as an empirical prior on random variable \mathcal{D}_t . While an adversary cannot see \mathcal{D}_t , the adversary’s goal is to use observable information to infer whether d_j is in \mathcal{D}_t ; if done with high certainty, the adversary is successful. While determining whether d_j is in \mathcal{D}_t is just one type of attack (a so-called membership inference attack (Shokri et al., 2017)), safety from membership inference under a public dataset serves as a proxy for safety from other attacks, in the sense that if an attacker cannot determine if d_j was used, the disclosure regarding d_j was limited.

Assume that \mathcal{D}_t is used to train some arbitrary model using the classical, mini-batch gradient descent (Alg. 1). The adversary uses some attack strategy \mathcal{F} to analyze the learned parameters θ_{N_r} to determine whether some d_j is in \mathcal{D}_t . We consider a worst-case (white-box) setting in which the model architecture and the released final parameters θ_{N_r} are known to the adversary.

Algorithm 1: Mini-Batch Stochastic Gradient Descent (SGD)

Input: Full dataset $\mathcal{D} = \{d_j\}_{j=1}^N$, parameterized model h_θ with parameter vector $\theta \in \mathbb{R}^{N_p}$, point-wise loss function $\ell[\theta, d]$, learning rate η , batch size B , number of training iterations N_r
Output: Optimized (final) model parameters θ_{N_r}
Initialize model parameters to θ_0 .
Sample a training set \mathcal{D}_t from \mathcal{D} according to sampling distribution $\mathcal{D}_t \sim Train(\mathcal{D})$.
Sample mini-batches $\{\mathcal{B}_i\}_{i=0}^{N_r-1}$ from \mathcal{D}_t according to sampling distribution $\{\mathcal{B}_i\} \sim Batch(\mathcal{D}_t)$.
for $i = 0$ **to** $N_r - 1$ **do**
 $\hat{g}_i = \frac{1}{B} \sum_{d_j \in \mathcal{B}_i} \nabla_\theta [\ell[\theta_i, d_j]]$
 $\theta_{i+1} = \theta_i - \eta \cdot \hat{g}_i$
end

We are now ready to define gradient uniqueness:

Definition 1. Consider training batch i . The *gradient uniqueness* of datapoint d_j with respect to batch i is given by:

$$GNQ_{ij} = g_{ij}^\top S^+ g_{ij} \quad (1)$$

where $S = \sum_{k=1, k \neq j}^N g_{ik} g_{ik}^\top \in \mathbb{R}^{N_p \times N_p}$ and S^+ denotes the Moore–Penrose pseudoinverse of S and $g_{ij} = \nabla_\theta [\ell[\theta_i, d_j]] \in \mathbb{R}^{N_p}$. Note that $S^+ = S^{-1}$ if S is invertible.

Then, the central result of the paper states that this quantity bounds the amount of information that any adversary can glean about d_j 's membership in \mathcal{D}_t by examining θ_{N_r} using \mathcal{F} :

Gradient uniqueness as an upper bound on disclosure (informal). *The amount of information (measured in bits) extracted by an adversary attempting to determine whether $d_j \in \mathcal{D}_t$ via examination of θ_{N_r} using any attack mechanism \mathcal{F} is upper-bounded by a function that increases monotonically with $\sum_{i=1}^{N_r-1} GNQ_{ij}$.*

A formal version of these results is given in Appendix A.

4 WHAT DOES GRADIENT UNIQUENESS MEASURE?

To show how GNQ measures privacy risk during gradient descent and to give some intuition behind the metric, we consider a simple example—a 2D linear regression model with the squared loss function (Fig. 1 a). The goal is to quantitatively rank the datapoints from the highest risk to the lowest risk.

The computation of GNQ can be geometrically represented as the construction of an ellipse summarizing the gradients; GNQ_{ij} is the extent to which the gradient associated with d_j is an outlier with respect to this ellipse, as shown in Fig. 1 b. In this figure, we plot the gradients of each of the seven training points, and the associated ellipses. Note that in the definition of GNQ_{ij} , the matrix S (and the resulting ellipse) is constructed using all the datapoints, except the point d_j for which GNQ_{ij} is computed. Thus there are two ellipses in Fig. 1 b: the blue ellipse is for the case when point 7 is excluded to compute GNQ_{i7} , while the red ellipse is for the case when point 7 is included while excluding one of the other six points to compute GNQ_{ik} where $k \in \{1, \dots, 6\}$. Datapoint 7 has a very high GNQ value because it falls outside of the blue ellipse, while all other datapoints have a low GNQ value, as they fall inside of the red ellipse.

Intuitively, as shown in Fig. 2, the gradients associated with points 1-6 want to rotate the regression line counter-clockwise, centered roughly on datapoint 5—whereas datapoint 7 is doing exactly the opposite, hence the high value for GNQ_{i7} .

GNQ-based auditing vs attack-based auditing. GNQ immediately suggests an auditing-based privacy scheme: monitor GNQ_{ij} for all training points, and if GNQ_{ij} is large and d_j is sensitive, take action, such as dropping d_j from the dataset, or unlearning d_j .

There are other auditing-based methods, the most well-known of which is MIA, which is an attack mechanism (see Sec. 2). MIA attempts to infer whether a given datapoint d_j was part of the training dataset. This goal is typically achieved by computing a membership score $\mathcal{M}[\theta_{N_r}, d_j]$ and comparing it against a decision threshold τ . Often the membership score is (or a function of) the model's loss on the target datapoint, while the decision threshold is a global threshold used for all datapoints determined either based on a heuristic (members ($d_j \in \mathcal{D}_t$) tend to have lower loss, while non-members ($d_j \notin \mathcal{D}_t$) tend to incur higher loss) or obtained by training shadow models.

In general, heuristic-based methods such as MIA produce very different results from GNQ. Consider Fig. 3. In gradient space, the global loss threshold $\ell = \tau$ appears as a horizontal strip bounded by the two lines $\partial\ell/\partial b = \pm\sqrt{2\tau}$. Points inside the strip ($|\partial\ell/\partial b| \leq \sqrt{2\tau}$) are classified as members in the training set; points outside are non-members. We consider two possible thresholds τ_1 and τ_2 . If we use τ_1 , points 2, 3, and 5 are inside the τ_1 -strip, so they will be ranked as high risk points, which does not match the GNQ ranking. Moreover, points 1, 4, 6 and 7 are outside the τ_1 -strip, so they will be classified safe points; this matches the GNQ ranking regarding points 1, 4, and 6, however it misranks point 7; the most crucial point in terms of privacy risk according to GNQ. Using τ_2 , points 2, 3, 5 and 7 are inside the τ_2 -strip, so they will be ranked as high risk points—which does not match the GNQ ranking except for point 7. Moreover, points 1, 4 and 6 are outside the τ_2 -strip, so they will be wrongly classified as low-disclosure points.

Further, any loss-based ranking depends solely on the residual (vertical distance to the fit), so points 2, 3, and 5—having smaller residuals (lower loss) than point 7—are necessarily ranked as higher risk for any choice of threshold. By contrast, $GNQ_{ij} = g_{ij}^\top S^{-1} g_{ij}$, uses the full gradient geometry: it accounts for (1) the residual r , (2) the feature vector (e.g., $[x, 1]$ in our 2D example)—both via the gradient formula $g = -r[x, 1]$ —and (3) inter-example correlations via S^{-1} .

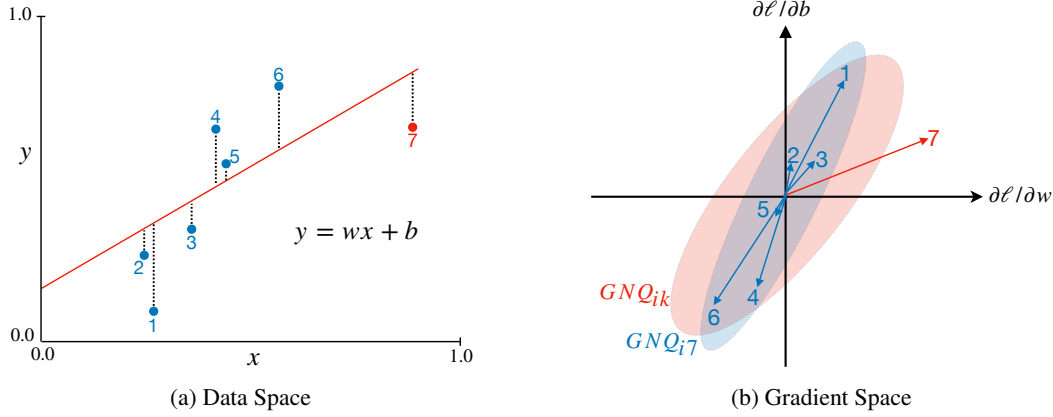


Figure 1: GNQ-based privacy auditing.

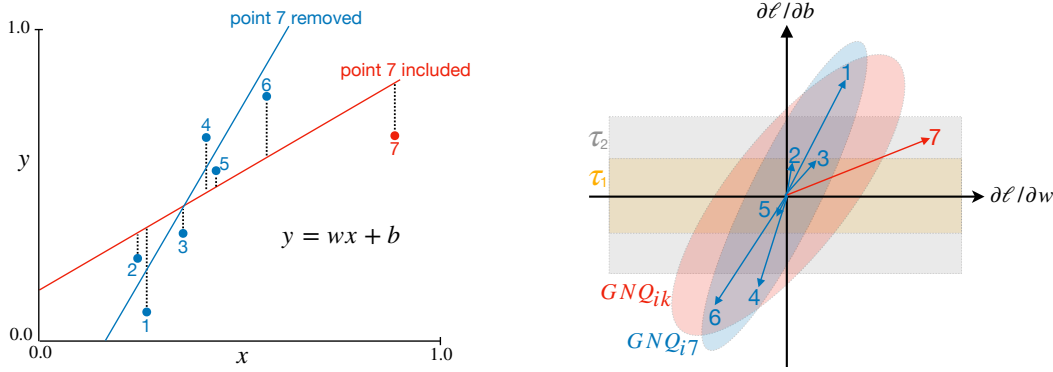


Figure 2: Accuracy of GNQ-based auditing.

Figure 3: GNQ vs. attack-based auditing.

5 A GNQ-BASED DEFENSE

While the central result of the paper is the definition and derivation of GNQ, we do wish to show that GNQ can be used to develop a simple defense; we leave other GNQ-based defenses to future work. The simple defense we consider consists of three steps: (i) train and rank datapoints within a dataset from the highest risk to the lowest risk using GNQ, (ii) remove the highest-risk points, and (iii) re-train using the filtered dataset.

For a smaller model with a limited number of parameters, the implementation is very straightforward. For a larger foundation model, implementing this simple GNQ-based defense requires some care, for several reasons. Most critical is the fact that the size of the matrix S scales quadratically with the number of model parameters, and inverting it is likely infeasible for a modern, large, model.

We can reduce the number of parameters that we have to consider by using a smaller, proxy model. That is, if the goal is to filter points before pre-training a 500B parameter model over a sensitive dataset, we can compute GNQ once at the end of a single training epoch using a 3B model in the same family. If this is still too expensive—and it is probably not reasonable to invert a $3B \times 3B$ matrix—we can rely on approximations of S^+ . The simplest is to compute only the diagonal of S and assume the off-diagonal elements are zero. It is this approximation we use in our experiments.

A final way to speed the computation is to only compute S using B gradients instead of N gradients. That is, when we compute the gradients over \mathcal{B}_i during gradient descent, for $d_j \in \mathcal{B}_i$, we compute GNQ_{ij} using $S = \sum_{\substack{d_k \in \mathcal{B}_i \\ k \neq j}} g_{ik} g_{ik}^\top$ instead of $S = \sum_{\substack{k=1 \\ k \neq j}}^N g_{ik} g_{ik}^\top$. This significantly reduces the number of gradient vectors that need to be memorized.

6 EXPERIMENTS

We evaluate on six datasets—MNIST (LeCun et al., 1998), CIFAR-10/100 (Krizhevsky, 2009), the AT&T Database of Faces (Samaria & Harter, 1994), Tiny ImageNet (Le & Yang, 2015; Deng et al., 2009), and IMDB (Maas et al., 2011)—using four model families: an MLP classifier, a basic CNN, ResNet (He et al., 2016) for vision, and a BERT-based classifier for text (Devlin et al., 2019). Models trained with Adam optimizer (Kingma & Ba, 2015).

6.1 GNQ-BASED DEFENSE

We begin by evaluating the utility of the simple, GNQ-based defense in the previous section.

MIA Experiment. We begin with a series of experiments that use a GNQ calculation—using the diagonalized S approximation—on a small version of a model in the same family (as described in Sec. 5), to filter out high-risk points. Our goal is to examine the privacy/model utility tradeoff obtained using this defense. Privacy is measured using the success of an MIA attack on the resulting model, to identify the points that were left out of the training set.

Specifically, we compute GNQ using a tiny CNN on CIFAR10, a tiny CNN on CIFAR100, a tiny ResNet on Tiny ImageNet, and a tiny BERT-based classifier on IMDB. Each tiny model is trained for a single epoch; we compute GNQ once at the end of that epoch. For each model-dataset pair, we remove the top- $p\%$ highest-risk points according to GNQ and retrain using the larger model. We also consider a non-private model (“Baseline”) and models trained with DP-SGD at $\epsilon \in \{2, 8, 512\}$.

Results. Table 1 shows both the AUC ROC obtained using a MIA (Salem et al., 2018), and the test accuracy obtained when using the learned model, after private training (or non-private training in the case of the baseline). For example, for CFAR100, we report how accurate is the resulting model in classifying test images.

These results show that it is possible to use the GNQ-based defense to push the attack AUC ROC roughly down to the level of random guessing, while obtaining significantly higher accuracy than what is obtained using DP-SGD.

ModInv Experiment. We train an MLP on AT&T Database of Faces. We rank examples by GNQ, and remove the single highest-GNQ-scored example (from class 6, the most vulnerable class by mean score), and retrain. We then apply the class-level ModInv attack of (Fredrikson et al., 2015) to class 6 before and after filtering.

Results. On the original dataset (95.31% validation accuracy), high-GNQ content is clearly reconstructed; after removing just one example, the filtered model (94.15% validation accuracy) substantially degrades reconstruction for the same class (Fig. 4).

6.2 CAN GRADIENT UNIQUENESS EXPLAIN WHAT’S OBSERVED IN PRACTICE?

In this section, we empirically validate the ability of GNQ to explain/predict empirical observations regarding the success rate of attacks, in terms of recovering a point or determining whether it was used in training, as well as observations regarding the impact of standard, algorithmic components of the SGD algorithm (batch size, learning rate, etc.) on the vulnerability of a learned model.

GNQ as an explanation for MIA success. We train four model-dataset pairs: a CNN on CIFAR10, a CNN on CIFAR100, a ResNet on Tiny ImageNet, and a BERT-based classifier on IMDB. For each trained model, we compute GNQ at the end of every epoch and summarize each example using the total GNQ. We then attack the learned model with the MIA of Salem et al. (2018) and record, per example, whether the attack succeeded. The goal is to see if there is a strong relationship between attack success and GNQ. To visualize the relation between our score and attack outcomes, we bin examples by GNQ on a logarithmic grid; the grey bars in Fig. 5 show the number of examples per bin. For each bin we compute the mean MIA success rate (blue curve).

Results. We find that across all models and datasets, the success rate increases with GNQ; examples with larger GNQ values are precisely those on which the attack is more likely to succeed.

GNQ as an explanation for ModInv success. We train two model-dataset pairs: an MLP on AT&T Database of Faces and a ResNet on MNIST. We then apply the class-level ModInv attack of

Table 1: Comparing GNQ-filtered SGD to DP-SGD for membership inference defense.

Dataset	Model	Setting	AUC ROC	Test Accuracy
CIFAR10	ResNet	Baseline	0.7294	80.80%
		Top-1% GNQ Removed	0.6896	77.98%
		Top-5% GNQ Removed	0.6002	73.66%
		Top-10% GNQ Removed	0.5122	71.33%
		DP-SGD ($\epsilon = 2$)	0.5008	41.83%
		DP-SGD ($\epsilon = 8$)	0.4998	47.18%
		DP-SGD ($\epsilon = 512$)	0.5030	55.99%
		Baseline	0.8752	49.58%
		Top-1% GNQ Removed	0.8213	46.19%
CIFAR100	ResNet	Top-5% GNQ Removed	0.8010	43.00%
		Top-10% GNQ Removed	0.6959	41.17%
		Top-15% GNQ Removed	0.6589	37.39%
		Top-20% GNQ Removed	0.5137	34.92%
		DP-SGD ($\epsilon = 2$)	0.5015	6.83%
		DP-SGD ($\epsilon = 8$)	0.5008	9.14%
		DP-SGD ($\epsilon = 512$)	0.5000	18.39%
		Baseline	0.9542	38.67%
		Top-1% GNQ Removed	0.9042	35.24%
Tiny ImageNet	ResNet	Top-5% GNQ Removed	0.8152	32.14%
		Top-10% GNQ Removed	0.7387	32.39%
		Top-15% GNQ Removed	0.6229	29.18%
		Top-20% GNQ Removed	0.5159	25.84%
		DP-SGD ($\epsilon = 2$)	0.4961	2.15%
		DP-SGD ($\epsilon = 8$)	0.4981	3.73%
		DP-SGD ($\epsilon = 512$)	0.5044	9.87%
		Baseline	0.7444	81.98%
		Top-0.5% GNQ Removed	0.5852	79.30%
IMDB	BERT	Top-1% GNQ Removed	0.6908	83.07%
		Top-5% GNQ Removed	0.4972	80.48%
		DP-SGD ($\epsilon = 2$)	0.4940	50.58%
		DP-SGD ($\epsilon = 8$)	0.4966	51.23%

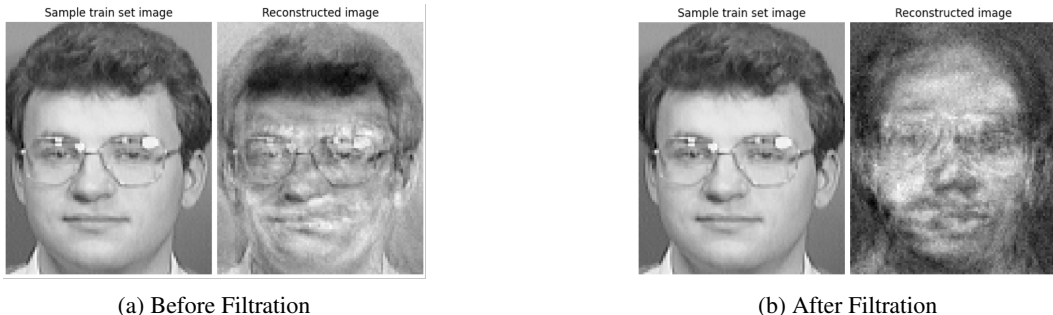


Figure 4: Image reconstruction after removing the highest-ranked image by GNQ.

(Fredrikson et al., 2015) on these trained models, to reconstruct the examples used during training. For each reconstructed image from a target class, we computed the minimum feature distance to any training example from that class. Feature distances were measured as the squared ℓ_2 norm between activations in the penultimate layer. A small feature distance corresponds to a successful attack, as the recovered image matches others in the class. Fig. 6 shows the relationship between GNQ and feature distance for each class (blue) across different models and datasets. The reported GNQ for a class is the sum of GNQ values of the individual examples, accumulated over all training iterations.

Results. The observed downward trend indicates a strong negative correlation between GNQ and feature distance, with Pearson correlation coefficients of $r = -0.90$ and $r = -0.96$. This trend

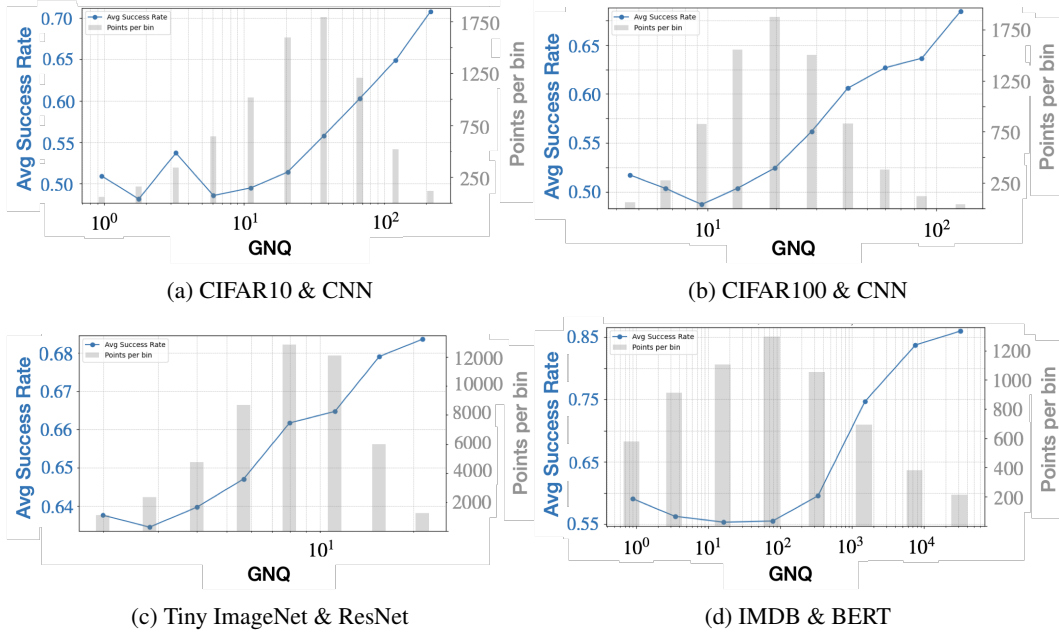


Figure 5: Attack success rate vs. GNQ.

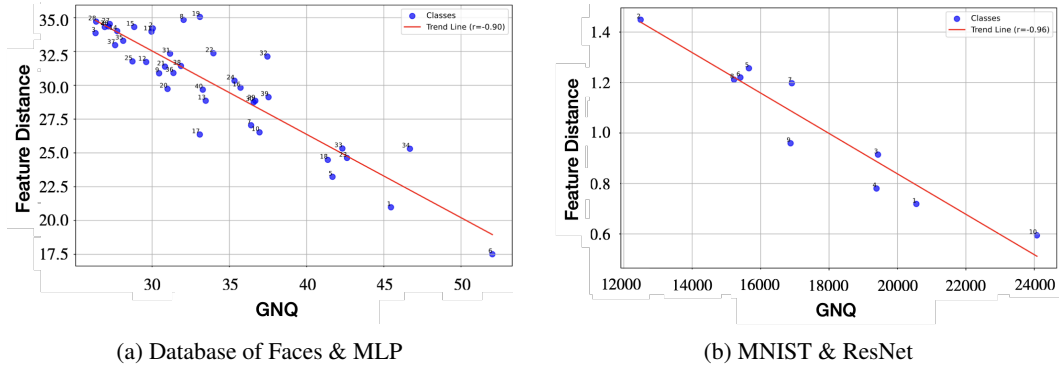


Figure 6: Feature distance vs. GNQ. Each blue circle represents a class.

suggests that classes with higher GNQ values tend to have smaller feature distances, meaning that reconstructed images are closer to real training samples. In Appendix B, we identified two classes of interest from the Database of Faces dataset: the class with the lowest GNQ (class 28) and the class with the highest GNQ (class 6).

GNQ as an explanation for SGD parameters and privacy. Finally, we demonstrate how GNQ can explain/predict the relationship between the privacy inherent to an SGD-style algorithm and the parameters used or chosen during training (dataset size, number of iterations, etc.) using the CIFAR-10 dataset with a CNN-based classifier. We consider one parameter setting at a time. For each setting, GNQ is computed for each training point at the end of each epoch, and we consider the maximum observed during training. The mean of the maximum values is used as a metric for the vulnerability of a particular parameter setting.

Results. We consider five parameters: the number of iterations (Fig. 7 a), the dataset size (Fig. 7 b), the model size (Fig. 7 c), the batch size (Fig. 7 d), and learning rate (Fig. 7 e). In each case, we plot the average-max GNQ value, as well as the MIA attack success rate (Salem et al., 2018) (MIA attack success is measured via AUC ROC). The results show that GNQ predicts, almost perfectly, how attack success will vary with various training parameters. However, it is important to note that these trends do not necessarily hold over all datasets and all attacks. While Fig. 7 a shows that

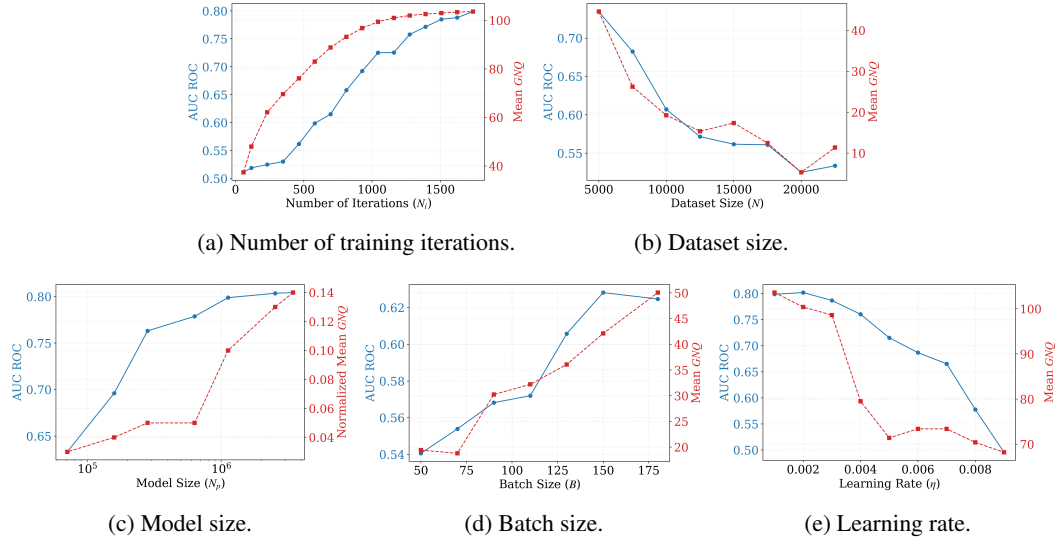


Figure 7: Relationship between various learning/dataset parameters, mean GNQ, and attack success (MIA attack, measured using AUC ROC) in the CIFAR-10 dataset. Plots show mean GNQ (right axis, red) and attack AUC ROC (left axis, blue).

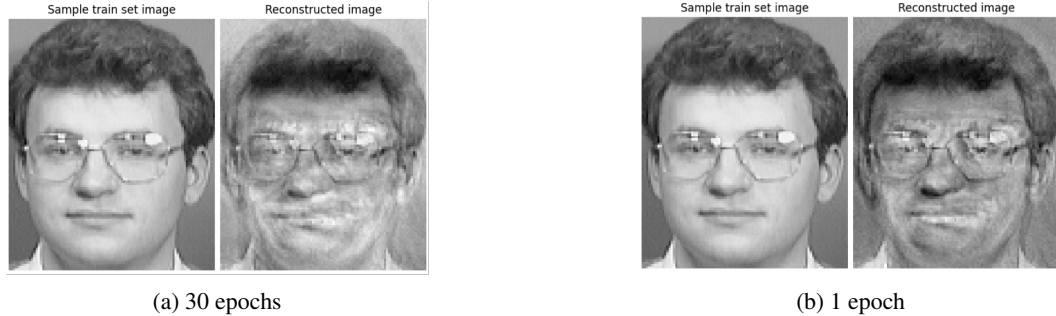


Figure 8: ModInv applied to the highest GNQ class in the Faces dataset. Reducing the number of epochs down to one fails to protect this class.

reducing the number of epochs affords some protection, it does not always afford this protection, and GNQ is able to determine vulnerable training points in an attack-agnostic way. We show, in Fig. 8, that even training for only a single epoch on the Faces dataset fails to protect high-GNQ classes from a reconstruction attack. Importantly, GNQ captures this vulnerability while being attack-agnostic.

7 CONCLUSION

We have derived a quantity called *gradient uniqueness* (GNQ) that increases monotonically with a bound on the information disclosure during mini-batch gradient descent. We have shown that indeed, GNQ strongly correlates with attack success. Future work should explore more sophisticated defenses based on GNQ. For example, one need not simply censor an entire datapoint with high GNQ, but could add a bit of noise to the gradient of a high-risk point, even adding noise only to certain dimensions of the gradient. GNQ may also serve emerging areas such as machine unlearning.

REFERENCES

Martin Abadi, Andy Chu, Ian Goodfellow, H. Brendan McMahan, Ilya Mironov, Kunal Talwar, and Li Zhang. Deep learning with differential privacy. In *Proceedings of the 2016 ACM SIGSAC Conference on Computer and Communications Security (CCS)*, pp. 308–318. ACM, 2016. doi: 10.1145/2976749.2978318.

Giuseppe Ateniese, Giovanni Felici, Luigi V. Mancini, Angelo Spognardi, Antonio Villani, and Domenico Vitali. Hacking smart machines with smarter ones: How to extract meaningful data from machine learning classifiers. *International Journal of Security and Networks*, 10(3):137–150, 2015. doi: 10.1504/IJSN.2015.071829.

Gilles Barthe, Boris Köpf, Federico Olmedo, and Santiago Zanella Béguelin. Probabilistic relational reasoning for differential privacy. In *Proceedings of the 39th ACM SIGPLAN-SIGACT Symposium on Principles of Programming Languages (POPL)*, pp. 97–110, 2012. doi: 10.1145/2103656.2103670.

Lucas Bourtoule, Varun Chandrasekaran, Christopher A. Choquette-Choo, Hengrui Jia, Adelin Travers, Baiwu Zhang, David Lie, and Nicolas Papernot. Machine unlearning. In *2021 IEEE Symposium on Security and Privacy (SP)*, pp. 141–159. IEEE, 2021. doi: 10.1109/SP40001.2021.00019.

Tom B. Brown, Benjamin Mann, Nick Ryder, Melanie Subbiah, Jared Kaplan, Prafulla Dhariwal, Arvind Neelakantan, Pranav Shyam, Girish Sastry, Amanda Askell, Sandhini Agarwal, Ariel Herbert-Voss, Gretchen Krueger, Tom Henighan, Rewon Child, Aditya Ramesh, Daniel M. Ziegler, Jeffrey Wu, Clemens Winter, Christopher Hesse, Mark Chen, Eric Sigler, Mateusz Litwin, Scott Gray, Benjamin Chess, Jack Clark, Christopher Berner, Sam McCandlish, Alec Radford, Ilya Sutskever, and Dario Amodei. Language models are few-shot learners, 2020. URL <https://arxiv.org/abs/2005.14165>.

Nicholas Carlini, Chang Liu, Jeremy Kos, Úlfar Erlingsson, and Shuang Song. Membership inference attacks from first principles. In *2022 IEEE Symposium on Security and Privacy (SP)*. IEEE, 2022.

Gilad Cohen and Raja Giryes. Membership inference attack using self influence functions. In *IEEE/CVF Winter Conference on Applications of Computer Vision (WACV)*, pp. 4892–4901, 2024.

Thomas M. Cover and Joy A. Thomas. *Elements of Information Theory (Wiley Series in Telecommunications and Signal Processing)*. Wiley-Interscience, USA, 2006. ISBN 0471241954.

Jia Deng, Wei Dong, Richard Socher, Li-Jia Li, Kai Li, and Li Fei-Fei. Imagenet: A large-scale hierarchical image database. In *Proc. CVPR*, pp. 248–255, 2009.

Jacob Devlin, Ming-Wei Chang, Kenton Lee, and Kristina Toutanova. Bert: Pre-training of deep bidirectional transformers for language understanding. In *Proc. NAACL-HLT*, 2019.

Cynthia Dwork and Aaron Roth. The algorithmic foundations of differential privacy. *Foundations and Trends in Theoretical Computer Science*, 9(3–4):211–407, 2014. doi: 10.1561/0400000042.

Cynthia Dwork, Frank McSherry, Kobbi Nissim, and Adam Smith. Calibrating noise to sensitivity in private data analysis. In *Theory of Cryptography Conference (TCC)*, volume 3876 of *LNCS*, pp. 265–284. Springer, 2006.

Matt Fredrikson, Somesh Jha, and Thomas Ristenpart. Model inversion attacks that exploit confidence information and basic countermeasures. In *Proceedings of the 22nd ACM SIGSAC Conference on Computer and Communications Security (CCS)*, pp. 1322–1333, 2015. doi: 10.1145/2810103.2813677.

Karan Ganju, Qi Wang, Wei Yang, Carl A. Gunter, and Nikita Borisov. Property inference attacks on fully connected neural networks using permutation invariant representations. In *Proceedings of the 2018 ACM SIGSAC Conference on Computer and Communications Security (CCS)*, pp. 619–633, 2018. doi: 10.1145/3243734.3243834.

Jonas Geiping, Hartmut Bauermeister, Hannah Dröge, and Michael Moeller. Inverting gradients—how easy is it to break privacy in federated learning? In *Advances in Neural Information Processing Systems (NeurIPS)*, 2020.

Gemini Google. Gemini: A family of highly capable multimodal models, 2025. URL <https://arxiv.org/abs/2312.11805>.

Aaron Grattafiori et al. The llama 3 herd of models, 2024. URL <https://arxiv.org/abs/2407.21783>.

Kaiming He, Xiangyu Zhang, Shaoqing Ren, and Jian Sun. Deep residual learning for image recognition. In *Proc. CVPR*, pp. 770–778, 2016.

Matthew Jagielski, Jonathan Ullman, and Alina Oprea. Auditing differentially private machine learning: How private is private sgd? In *Advances in Neural Information Processing Systems (NeurIPS)*, volume 33, pp. 22205–22216, 2020.

Mishaal Kazmi, Hadrien Lautraite, Alireza Akbari, Qiaoyue Tang, Mauricio Soroco, Tao Wang, Sébastien Gambs, and Mathias Lécuyer. Panoramia: Privacy auditing of machine learning models without retraining. *arXiv preprint arXiv:2402.09477*, 2024. doi: 10.48550/arXiv.2402.09477. URL <https://arxiv.org/abs/2402.09477>.

Diederik P. Kingma and Jimmy Ba. Adam: A method for stochastic optimization. In *Proc. ICLR*, 2015.

Alex Krizhevsky. Learning multiple layers of features from tiny images. Technical report, University of Toronto, 2009.

Ya Le and Xuan S. Yang. Tiny imagenet visual recognition challenge, 2015. Stanford CS231n course project.

Yann LeCun, Léon Bottou, Yoshua Bengio, and Patrick Haffner. Gradient-based learning applied to document recognition. *Proceedings of the IEEE*, 86(11):2278–2324, 1998.

Andrew L. Maas, Raymond E. Daly, Peter T. Pham, Dan Huang, Andrew Y. Ng, and Christopher Potts. Learning word vectors for sentiment analysis. In *Proceedings of the 49th Annual Meeting of the Association for Computational Linguistics: Human Language Technologies*, pp. 142–150, 2011.

Beren Millidge and Eric Winsor. Basic facts about language model internals. *AI Alignment Forum*, January 2023. URL <https://www.alignmentforum.org/posts/PDLfpRwSynu73mxGw/basic-facts-about-language-model-internals-1>. Accessed: 2025-09-22.

Sasi Kumar Murakonda and Reza Shokri. MI privacy meter: Aiding regulatory compliance by quantifying the privacy risks of machine learning. In *HotPETs (Workshop on Hot Topics in Privacy Enhancing Technologies)*, 2020. URL <https://crysdpetsymposium.org/2020/files/hotpets/MLPrivacyMeter.pdf>.

Sasi Kumar Murakonda, Reza Shokri, and George Theodorakopoulos. Quantifying the privacy risks of learning high-dimensional graphical models, 2021. URL <https://arxiv.org/abs/1905.12774>.

Milad Nasr, Reza Shokri, and Amir Houmansadr. Comprehensive privacy analysis of deep learning: Passive and active white-box inference attacks against centralized and federated learning. In *2019 IEEE Symposium on Security and Privacy (SP)*, pp. 739–753. IEEE, 2019. doi: 10.1109/SP.2019.00065.

Milad Nasr, Jamie Hayes, Thomas Steinke, Borja Balle, Florian Tramèr, Matthew Jagielski, Nicholas Carlini, and Andreas Terzis. Tight auditing of differentially private machine learning. In *32nd USENIX Security Symposium (USENIX Security 23)*, 2023. URL <https://www.usenix.org/system/files/usenixsecurity23-nasr.pdf>.

Maria-Irina Nicolae, Mathieu Sinn, Minh Ngoc Tran, Beat Buesser, Ambrish Rawat, Martin Wistuba, Valentina Zantedeschi, Nathalie Baracaldo, Bryant Chen, Heiko Ludwig, Ian M. Molloy, and Ben Edwards. Adversarial robustness toolbox v1.0.0. *arXiv preprint arXiv:1807.01069*, 2018. URL <https://arxiv.org/abs/1807.01069>.

OpenDP. *opendp: R Bindings for the OpenDP Library*, 2025. URL <https://opendp.org/>. R package version 0.13.0.

Abhishek Panigrahi, Raghav Soman, Navin Goyal, and Praneeth Netrapalli. Non-gaussianity of stochastic gradient noise, 2019. URL <https://arxiv.org/abs/1910.09626>.

Alec Radford, Jeffrey Wu, Rewon Child, David Luan, Dario Amodei, and Ilya Sutskever. Language models are unsupervised multitask learners. Technical report, OpenAI, 2019. URL https://cdn.openai.com/better-language-models/language_models_are_unsupervised_multitask_learners.pdf.

Alexandre Sablayrolles, Matthijs Douze, Yann Ollivier, Cordelia Schmid, and Hervé Jégou. White-box vs black-box: Bayes optimal strategies for membership inference, 2019. URL <https://arxiv.org/abs/1908.11229>.

Ahmed Salem, Yang Zhang, Mathias Humbert, Pascal Berrang, Mario Fritz, and Michael Backes. ML-Leaks: Model and data independent membership inference attacks and defenses on machine learning models. *arXiv preprint arXiv:1806.01246*, 2018.

F. S. Samaria and A. C. Harter. Parameterisation of a stochastic model for human face identification. In *Proceedings of 1994 IEEE Workshop on Applications of Computer Vision*, pp. 138–142, 1994.

Reza Shokri, Marco Stronati, Congzheng Song, and Vitaly Shmatikov. Membership inference attacks against machine learning models. In *2017 IEEE Symposium on Security and Privacy (SP)*, pp. 3–18. IEEE, 2017. doi: 10.1109/SP.2017.41.

David Marco Sommer, Liwei Song, Sameer Wagh, and Prateek Mittal. Athena: Probabilistic verification of machine unlearning. *Proceedings on Privacy Enhancing Technologies (PoPETs)*, 2022 (4):268–290, 2022.

Liwei Song and Prateek Mittal. Systematic evaluation of privacy risks of machine learning models. In *30th USENIX Security Symposium (USENIX Security 21)*, 2021. URL <https://www.usenix.org/system/files/sec21fall-song.pdf>.

Thomas Steinke, Borja Balle, Matthew Jagielski, Janardhan Kulkarni, Milad Nasr, and Florian Tramer. Privacy auditing with one training run. In *Advances in Neural Information Processing Systems (NeurIPS)*, 2023.

Trail of Bits. Privacyraven: Privacy testing for deep learning. <https://github.com/trailofbits/PrivacyRaven>, 2021.

Aleksi Triastcyn and Boi Faltings. Bayesian differential privacy for machine learning, 2020. URL <https://arxiv.org/abs/1901.09697>.

VaultGemma. VaultGemma: A differentially private Gemma model. Technical report, Google Research and Google DeepMind, September 2025. URL https://services.google.com/fh/files/blogs/vaultgemma_tech_report.pdf.

Zihan Wang, Jason D. Lee, and Qi Lei. Reconstructing training data from model gradient, provably, 2023. URL <https://arxiv.org/abs/2212.03714>.

Alexander Warnecke, Lukas Pirch, Christian Wressnegger, and Konrad Rieck. Machine unlearning of features and labels. In *Network and Distributed System Security Symposium (NDSS)*, 2023.

Lauren Watson, Chuan Guo, Graham Cormode, and Alex Sablayrolles. On the importance of difficulty calibration in membership inference attacks, 2022. URL <https://arxiv.org/abs/2111.08440>.

Jiayuan Ye, Aadyaa Maddi, Sasi Kumar Murakonda, Vincent Bindschaedler, and Reza Shokri. Enhanced membership inference attacks against machine learning models, 2022. URL <https://arxiv.org/abs/2111.09679>.

Danfeng Zhang and Daniel Kifer. Lightdp: Towards automating differential privacy proofs. In *Proceedings of the 44th ACM SIGPLAN Symposium on Principles of Programming Languages (POPL)*, 2017.

Ligeng Zhu, Zhijian Liu, and Song Han. Deep leakage from gradients. In *Advances in Neural Information Processing Systems (NeurIPS)*. Curran Associates, Inc., 2019. URL <https://arxiv.org/abs/1906.08935>.

A GRADIENT UNIQUENESS AS A MEASURE OF DATA PRIVACY

A.1 OVERVIEW

In this section, we argue that gradient uniqueness is a practical and effective measure for quantifying data privacy. It is straightforward to construct adversarial scenarios where the inclusion of a single datapoint in a training set can be inferred from a trained model. Consequently, it is impossible to formulate a general theorem that guarantees protection against such membership inference attacks in all cases.

However, there is a consensus among practitioners that such worst-case scenarios are unlikely to occur in practice. Our objective is to bridge the gap between this practical intuition and theoretical guarantees. We show that under common practical assumptions, the gradient uniqueness measure rigorously quantifies the risk of an adversary successfully inferring the membership of a specific datapoint.

Our argument is grounded in information theory (Cover & Thomas, 2006). Our result shows that under some practical assumptions, the randomness in the mini-batch SGD (Algorithm 1) provides some level of protection for the membership of the datapoint d_j in the training dataset \mathcal{D}_t denoted by T_j . It is well-known that if the mutual information between a target variable, say T_j , and an observable variable is small, then no algorithm can predict T_j with a success probability significantly better than a random guess (i.e., 50%). We formally demonstrate that the mutual information between the membership variable T_j and the released model is *upper-bounded by an increasing function of gradient uniqueness*. This result provides a firm theoretical justification for using gradient uniqueness as a proxy for the information leakage associated with a particular datapoint.

Problem setup: Before stating our core argument, we recall the setup of our problem and Algorithm 1. To simplify our analysis, we define the sampling distributions $Train()$ and $Batch()$ as follows. For each datapoint d_j , let $T_j \sim Ber(N_t/N)$ control whether d_j is included in \mathcal{D}_t . Assume $N_t = N/2$. For training batch i , let $M_{i,j} \sim Ber(B/N_t)$ be a random variable controlling whether d_j is included in the mini-batch. In particular, we include the datapoint d_j in the batch if and only if $T_j \cdot M_{i,j} = 1$. All these Bernoulli random variables are drawn independently.

We denote the gradient of the loss function at iteration i , evaluated at datapoint d_j , by

$$g_{i,j} := \nabla_{\theta} \ell(\theta_i, d_j).$$

The mini-batch gradient is defined as the average of these gradients, normalized by B (the expected batch size) rather than the realized batch size:

$$\hat{g}_i := \frac{1}{B} \sum_{j=1}^N T_j \cdot M_{i,j} \cdot g_{i,j} = \frac{1}{B} \sum_{j=1}^N T_j \cdot M_{i,j} \cdot \nabla_{\theta} \ell(\theta_i, d_j).$$

The SGD algorithm runs in N_r iterations with the following update rule:

$$\theta_{i+1} = \theta_i - \eta \cdot \hat{g}_i,$$

where η is a fixed step size. The initial model θ_0 is chosen independently of the dataset; equivalently, for all T_j , we have $I[T_j; \theta_0] = 0$.

We emphasize that there is no randomness in the overall dataset \mathcal{D} ; that is the set of all possible datapoints is known to everyone. The training set, however, is a random subset of \mathcal{D} . The fact that a particular datapoint is used or not is a quantity that we would like to protect.

Our assumptions: Our subsequent theoretical development hinges on two main assumptions that do not hold in general. However, these assumptions are motivated by empirical observations about the SGD algorithm.

- Gradients are often empirically observed to resemble Gaussian distributions (Panigrahi et al., 2019; Millidge & Winsor, 2023). Motivated by this observation, we assume that the entropy of the batch gradients can be approximated by that of a multivariate normal distribution with the same covariance structure. For a formal statement, see Equation 3.

- We assume that in each iteration the gradients measured at individual datapoints $g_{i,j}$ reside within the same subspace spanned by the rest of the data $\{g_{i,j'}\}_{j \neq j'}$. In other words, there are no outlier points whose gradients drive the model in directions unique to themselves.

A.2 GRADIENT UNIQUENESS AS AN UPPER BOUND ON DISCLOSURE

In this section, we utilize the assumptions of the prior section to argue that gradient uniqueness is a practical bound on information disclosure. Various theorems and lemmas used in our argument are given in Sec. A.3.

As stated, our goal is to define a proxy that captures an attacker’s ability to infer T_j from the final model θ_{N_r} . Prior to training, an adversary only knows that $T_j \sim \text{Ber}(B/N_t)$, yielding a trivial baseline guess. The mutual information then quantifies how much this baseline can be improved when the adversary observes θ_{N_r} .

We begin by decomposing the mutual information between T_j and the final model θ_{N_r} and relate it to the entropy of the mini-batch gradients using information-theoretic tools. In particular, we will rely on the following theorem. The proof of this theorem is provided in Sec. A.3.

Theorem A.1. *In mini-batch SGD (Algorithm 1), for any $j \in [N]$ and corresponding datapoint $d_j \in \mathcal{D}$, the mutual information between its training membership indicator $T_j \in \{0, 1\}$ and the estimate $\hat{T}_j := \mathcal{F}(\theta_{N_r}, j)$ produced by an attacker \mathcal{F} is bounded by:*

$$\begin{aligned} & I[T_j; \mathcal{F}(\theta_{N_r}, j)] \\ & \leq \sum_{i=1}^{N_r-1} H[\hat{g}_i \mid \theta_i] - H[\hat{g}_i \mid \theta_i, T_j = 0] - \frac{N_t}{N} \cdot \left(H[\hat{g}_i \mid \theta_i, T_j = 1] - H[\hat{g}_i \mid \theta_i, T_j = 0] \right). \end{aligned} \quad (2)$$

Given this theorem, we now use our assumption that the distribution of \hat{g}_i resembles a (possibly degenerate) multivariate normal distribution to approximate its entropy as:

$$H[\hat{g}_i \mid \theta_i] \approx \frac{1}{2} \log((2\pi e)^r \text{pdet}(\Sigma)), \quad (3)$$

where Σ denotes the covariance matrix of \hat{g}_i conditioned on θ_i , $\text{pdet}(\Sigma)$ is the pseudo-determinant of Σ (the product of its nonzero eigenvalues), and $r = \text{rank}(\Sigma)$. Similarly, we define $\Sigma^{(j,0)}$ (resp. $\Sigma^{(j,1)}$) as the covariance matrix of \hat{g}_i conditioned on θ_i and $T_j = 0$ (resp. $T_j = 1$). We derive these covariance matrices explicitly in Sec. A.4. As we show, the matrices are given by:

$$\begin{aligned} \Sigma &= \frac{1}{BN} \cdot \left(1 - \frac{B}{N} \right) \sum_{j=1}^N g_{i,j} g_{i,j}^\top \\ \Sigma^{(j,0)} &= \frac{1}{BN} \cdot \left(1 - \frac{B}{N} \right) \sum_{j' \neq j} g_{i,j'} g_{i,j'}^\top \\ \Sigma^{(j,1)} &= \frac{1}{BN_t} \cdot \left(1 - \frac{B}{N_t} \right) \cdot g_{i,j} g_{i,j}^\top + \frac{1}{BN} \cdot \left(1 - \frac{B}{N} \right) \sum_{j' \neq j} g_{i,j'} g_{i,j'}^\top. \end{aligned}$$

It is not hard to see that Σ and $\Sigma^{(j,1)}$ are rank-one perturbation of $\Sigma^{(j,0)}$. In particular, we have:

$$\begin{aligned} \Sigma &= \Sigma^{(j,0)} + \underbrace{\frac{1}{BN} \cdot \left(1 - \frac{B}{N} \right) \cdot g_{i,j} g_{i,j}^\top}_{c_1^2 :=} \\ \Sigma^{(j,1)} &= \Sigma^{(j,0)} + \underbrace{\frac{1}{BN_t} \cdot \left(1 - \frac{B}{N_t} \right) \cdot g_{i,j} g_{i,j}^\top}_{c_2^2 :=}. \end{aligned}$$

Let us define $q = c_1 g_{i,j}$ and $q' = c_2 g_{i,j}$ where c_1 and c_2 are the constant we have above. Note that earlier we assumed that $g_{i,j}$ belongs to the span of $\{g_{i,j'}\}_{j \neq j'}$. In Lemma A.2, we show that q and q' must have belong to the range of $\Sigma^{(j,0)}$. Furthermore, in Lemma A.3 we show that adding qq^\top (or $q'q'^\top$) does not change rank of $\Sigma^{(j,0)}$. Our assumptions lead to a clean approximation of the right hand side of Equation 2. In particular, we have the following bound via Theorem A.1:

$$\begin{aligned}
 & I[T_j; \mathcal{F}(\theta_{N_r}, j)] \\
 & \leq \sum_{i=1}^{N_r-1} H[\hat{g}_i \mid \theta_i] - H[\hat{g}_i \mid \theta_i, T_j = 0] - \frac{N_t}{N} \cdot \left(H[\hat{g}_i \mid \theta_i, T_j = 1] - H[\hat{g}_i \mid \theta_i, T_j = 0] \right) \\
 & \approx \sum_{i=1}^{N_r-1} \frac{1}{2} \left(\log \left(\frac{\text{pdet}(\Sigma)}{\text{pdet}(\Sigma^{(j,0)})} \right) - \frac{N_t}{N} \log \left(\frac{\text{pdet}(\Sigma^{(j,1)})}{\text{pdet}(\Sigma^{(j,0)})} \right) \right) \\
 & = \sum_{i=1}^{N_r-1} \frac{1}{2} \left(\log \left(1 + c_1^2 g_{i,j}^\top (\Sigma^{(j,0)})^+ g_{i,j} \right) - \frac{N_t}{N} \log \left(1 + c_2^2 g_{i,j}^\top (\Sigma^{(j,0)})^+ g_{i,j} \right) \right) \\
 & = \sum_{i=1}^{N_r-1} \frac{1}{2} \left(\log \left(\frac{1 + c_1^2 g_{i,j}^\top (\Sigma^{(j,0)})^+ g_{i,j}}{(1 + c_2^2 g_{i,j}^\top (\Sigma^{(j,0)})^+ g_{i,j})^{N_t/N}} \right) \right).
 \end{aligned}$$

Assuming that $N_t = N/2$, what we have in the last line is an increasing function of $x := g_{i,j}^\top (\Sigma^{(j,0)})^+ g_{i,j}$. We prove this by showing that

$$f(x) := \frac{1 + c_1^2 x}{\sqrt{1 + c_2^2 x}}$$

is an increasing function of x in Lemma A.4 for our desired range of parameters. This completes the argument that gradient uniqueness serves as a practical upper bound on the information available to an attacker on whether $T_j = 1$.

A.3 PROOFS OF THEOREMS AND LEMMAS

Theorem A.1. *In mini-batch SGD (Algorithm 1), for any $j \in [N]$ and corresponding datapoint $d_j \in \mathcal{D}$, the mutual information between its training membership indicator $T_j \in \{0, 1\}$ and the estimate $\hat{T}_j := \mathcal{F}(\theta_{N_r}, j)$ produced by an attacker \mathcal{F} is bounded by:*

$$\begin{aligned}
 & I[T_j; \mathcal{F}(\theta_{N_r}, j)] \\
 & \leq \sum_{i=1}^{N_r-1} H[\hat{g}_i \mid \theta_i] - H[\hat{g}_i \mid \theta_i, T_j = 0] - \frac{N_t}{N} \cdot \left(H[\hat{g}_i \mid \theta_i, T_j = 1] - H[\hat{g}_i \mid \theta_i, T_j = 0] \right). \tag{2}
 \end{aligned}$$

Proof. Fix $j \in [N]$ for the rest of the proof. Note that using the SGD update rule, the final model θ_{N_r} is obtained from the second to last model θ_{N_r-1} together with the gradient in the last batch \hat{g}_{N_r-1} . By the data processing inequality, we obtain:

$$\begin{aligned}
 I[T_j; \mathcal{F}(\theta_{N_r}, j)] & \leq I[T_j; \theta_{N_r}] \leq I[T_j; \theta_{N_r-1}, \hat{g}_{N_r-1}] \\
 & = I[T_j; \theta_{N_r-1}] + I[T_j; \hat{g}_{N_r-1} \mid \theta_{N_r-1}] \tag{via chain rule}
 \end{aligned}$$

By recursively applying this decomposition from step N_r down to step 0, we obtain:

$$I[T_j; \mathcal{F}(\theta_{N_r}, j)] \leq I[T_j; \theta_0] + \sum_{i=1}^{N_r-1} I[T_j; \hat{g}_i \mid \theta_i].$$

Since the initial model θ_0 is chosen independently of the training data, we have $I[T_j; \theta_0] = 0$. Hence, we obtain:

$$I[T_j; \mathcal{F}(\theta_{N_r}, j)] \leq \sum_{i=1}^{N_r-1} I[T_j; \hat{g}_i | \theta_i]. \quad (4)$$

We now analyze each term in the above summation. By definition of mutual information and the conditional entropy, we have

$$\begin{aligned} I[T_j; \hat{g}_i | \theta_i] &= H[\hat{g}_i | \theta_i] - H[\hat{g}_i | \theta_i, T_j] \\ &= H[\hat{g}_i | \theta_i] - \mathbb{P}[T_j = 0] \cdot H[\hat{g}_i | \theta_i, T_j = 0] - \mathbb{P}[T_j = 1] \cdot H[\hat{g}_i | \theta_i, T_j = 1] \\ &= H[\hat{g}_i | \theta_i] - \left[1 - \frac{N_t}{N}\right] \cdot H[\hat{g}_i | \theta_i, T_j = 0] - \left[\frac{N_t}{N}\right] \cdot H[\hat{g}_i | \theta_i, T_j = 1] \\ &= H[\hat{g}_i | \theta_i] - H[\hat{g}_i | \theta_i, T_j = 0] - \frac{N_t}{N} \cdot (H[\hat{g}_i | \theta_i, T_j = 1] - H[\hat{g}_i | \theta_i, T_j = 0]) \end{aligned} \quad (5)$$

Here we used that T_j is a Bernoulli random variable with parameter N_t/N . Substituting Equation 5 into Equation 4 yields the stated bound, completing the proof. \square

Lemma A.2. *Let $x_1, \dots, x_n \in \mathbb{R}^d$ (not necessarily linearly independent) and define*

$$A = \sum_{i=1}^n x_i x_i^\top \in \mathbb{R}^{d \times d}.$$

Then $\text{Range}(A) = \text{span}\{x_1, \dots, x_n\}$. In particular, each x_i lies in $\text{Range}(A)$.

Proof. First, for any $y \in \mathbb{R}^d$ we have

$$Ay = \sum_{i=1}^n x_i (x_i^\top y) \in \text{span}\{x_1, \dots, x_n\},$$

so $\text{Range}(A) \subseteq \text{span}\{x_1, \dots, x_n\}$.

For the reverse inclusion, observe that A is symmetric positive semidefinite, and its nullspace is

$$\mathcal{N}(A) = \{y \in \mathbb{R}^d : Ay = 0\} = \{y \in \mathbb{R}^d : x_i^\top y = 0 \text{ for all } i\},$$

since $y^\top Ay = \sum_{i=1}^n (x_i^\top y)^2 = 0$ iff $x_i^\top y = 0$ for all i . Therefore $\mathcal{N}(A) = \text{span}\{x_1, \dots, x_n\}^\perp$. By the Fundamental Theorem of Linear Algebra,

$$\text{Range}(A) = \mathcal{N}(A)^\perp = (\text{span}\{x_1, \dots, x_n\}^\perp)^\perp = \text{span}\{x_1, \dots, x_n\}.$$

Hence each $x_i \in \text{Range}(A)$. \square

Lemma A.3. *Let $A \in \mathbb{R}^{n \times n}$ be a symmetric matrix (not necessarily full-rank), and let $q \in \text{range}(A)$. Then*

$$\text{pdet}(A + qq^\top) = \text{pdet}(A) (1 + q^\top A^+ q),$$

where $\text{pdet}(\cdot)$ denotes the pseudo-determinant (the product of the nonzero eigenvalues) and A^+ is the Moore–Penrose pseudoinverse. Moreover, the rank of A and $A + qq^\top$ are the same.

Proof. Since A is symmetric, by the spectral theorem we may write

$$A = \sum_{i=1}^r \lambda_i u_i u_i^\top,$$

where $\lambda_1, \dots, \lambda_r \neq 0$ are the nonzero eigenvalues of A , u_1, \dots, u_r are the corresponding orthonormal eigenvectors, and the remaining eigenvalues are zero. Equivalently,

$$A = U \begin{bmatrix} \Lambda_r & 0 \\ 0 & 0 \end{bmatrix} U^\top,$$

where $U = [U_r \ U_0]$ is orthogonal, $\Lambda_r = \text{diag}(\lambda_1, \dots, \lambda_r)$, and $\text{range}(A) = \text{span}(U_r)$.

Since $q \in \text{range}(A)$, we can write $q = U_r y$ for some $y \in \mathbb{R}^r$. Then

$$A + qq^\top = U \begin{bmatrix} \Lambda_r + yy^\top & 0 \\ 0 & 0 \end{bmatrix} U^\top.$$

The nonzero spectrum of $A + qq^\top$ is the nonzero spectrum of $\Lambda_r + yy^\top$.¹ Note that since Λ_r is positive definite and yy^\top is positive semi-definite, their sum $\Lambda_r + yy^\top$ is also positive definite. It is therefore full rank and has a non-zero determinant. This representation also implies that the number of orthonormal eigenvectors with nonzero eigenvalues does not change after perturbation, meaning that the ranks of A and $A + qq^\top$ are the same. Moreover, we have:

$$\text{pdet}(A + qq^\top) = \det(\Lambda_r + yy^\top).$$

Applying the matrix determinant lemma implies

$$\det(\Lambda_r + yy^\top) = \det(\Lambda_r) (1 + y^\top \Lambda_r^{-1} y).$$

Now note that

$$\det(\Lambda_r) = \text{pdet}(A), \quad y^\top \Lambda_r^{-1} y = q^\top A^+ q,$$

where $A^+ = U_r \Lambda_r^{-1} U_r^\top$ is the Moore–Penrose pseudoinverse of A .

Therefore,

$$\text{pdet}(A + qq^\top) = \text{pdet}(A) (1 + q^\top A^+ q),$$

as claimed. \square

Lemma A.4. *Let $c_1, c_2 > 0$ and, for $x \geq 0$, define*

$$f(x) := \frac{1 + c_1^2 x}{\sqrt{1 + c_2^2 x}}.$$

If $2c_1^2 > c_2^2$, then f is an increasing function of x on $[0, \infty)$.

Proof. For $x \geq 0$,

$$f(x) = (1 + c_1^2 x) (1 + c_2^2 x)^{-1/2},$$

so by the product/chain rules,

$$f'(x) = c_1^2 (1 + c_2^2 x)^{-1/2} - \frac{1}{2} (1 + c_1^2 x) c_2^2 (1 + c_2^2 x)^{-3/2} = \frac{(2c_1^2 - c_2^2) + c_1^2 c_2^2 x}{2(1 + c_2^2 x)^{3/2}}.$$

The denominator is positive for all $x \geq 0$. Under $2c_1^2 > c_2^2$ the numerator is positive for all $x \geq 0$. Hence $f'(x) > 0$ on $[0, \infty)$, so f is an increasing function of x on this interval. \square

A.4 DERIVATION OF COVARIANCE MATRICES

Recall that we define Σ to be the covariance matrix of \hat{g}_i conditioned on θ_i . Our derivation begins by calculating the (a, b) entry of the Σ , and expanding it. In the following, we use $g_{i,j}^{(a)}$ to denote the a th coordinate of the vector $g_{i,j}$.

$$\Sigma_{ab} = \frac{1}{B^2} \cdot \text{cov} \left(\sum_{j=1}^N T_j M_{i,j} g_{i,j}^{(a)}, \sum_{j'=1}^N T_{j'} M_{i,j'} g_{i,j'}^{(b)} \right)$$

By the definition of covariance, this can be written as:

$$\Sigma_{ab} = \frac{1}{B^2} \cdot \left(E \left[\left(\sum_{j=1}^N T_j M_{i,j} g_{i,j}^{(a)} \right) \left(\sum_{j'=1}^N T_{j'} M_{i,j'} g_{i,j'}^{(b)} \right) \right] - E \left[\sum_{j=1}^N T_j M_{i,j} g_{i,j}^{(a)} \right] E \left[\sum_{j'=1}^N T_{j'} M_{i,j'} g_{i,j'}^{(b)} \right] \right).$$

¹If $A = UBU^{-1}$ with U invertible, then w is an eigenvector of B with eigenvalue λ iff $U^{-1}w$ is an eigenvector of A with the same eigenvalue λ .

Rearranging the sums and expectations gives:

$$\Sigma_{ab} = \frac{1}{B^2} \cdot \sum_{j,j'=1}^N (E[T_j M_{i,j} T_{j'} M_{i,j'}] - E[T_j M_{i,j}] E[T_{j'} M_{i,j'}]) g_{i,j}^{(a)} g_{i,j}^{(b)}$$

This simplifies to a sum of covariances:

$$\Sigma_{ab} = \frac{1}{B^2} \cdot \sum_{j,j'=1}^N \text{cov}(T_j M_{i,j}, T_{j'} M_{i,j'}) g_{i,j}^{(a)} g_{i,j'}^{(b)}$$

Given that for $j \neq j'$, the terms $T_j M_{i,j}$ and $T_{j'} M_{i,j'}$ are independent, their covariance is zero. This eliminates the terms where $j \neq j'$, leaving only the terms where $j = j'$:

$$\begin{aligned} \Sigma_{ab} &= \frac{1}{B^2} \cdot \sum_{j=1}^N \text{cov}(T_j M_{i,j}, T_j M_{i,j}) g_{i,j}^{(a)} g_{i,j}^{(b)} \\ &= \frac{1}{B^2} \cdot \sum_{j=1}^N \text{var}(T_j M_{i,j}) g_{i,j}^{(a)} g_{i,j}^{(b)} \\ &= \frac{1}{B^2} \cdot \sum_{j=1}^N \frac{B}{N} \cdot \left(1 - \frac{B}{N}\right) g_{i,j}^{(a)} g_{i,j}^{(b)} \\ &= \frac{1}{B N} \cdot \left(1 - \frac{B}{N}\right) \sum_{j=1}^N g_{i,j}^{(a)} g_{i,j}^{(b)}. \end{aligned}$$

In the above calculation, we use that $T_j M_{i,j}$ can be viewed as a Bernoulli random variable with parameter $\frac{N_t}{N} \cdot \frac{B}{N_t} = \frac{B}{N}$. Writing Σ in the matrix form give us:

$$\Sigma = \frac{1}{B N} \cdot \left(1 - \frac{B}{N}\right) \sum_{j=1}^N g_{i,j} g_{i,j}^\top. \quad (6)$$

Next, we compute $\Sigma^{(j,0)}$ and $\Sigma^{(j,1)}$ similarly for a fixed j . Condition on $T_j = 0$, $T_j \cdot M_{i,j}$ is always zero, so the variance is zero. Thus, we have:

$$\Sigma^{(j,0)} = \frac{1}{B N} \cdot \left(1 - \frac{B}{N}\right) \sum_{j' \neq j} g_{i,j'} g_{i,j'}^\top. \quad (7)$$

Condition on T_j being one, $T_j \cdot M_{i,j}$ is equal to $M_{i,j}$, a Bernoulli random variable with variance $(B/N_t) \cdot (1 - B/N_t)$. Thus, we have:

$$\Sigma^{(j,1)} = \frac{1}{B N_t} \cdot \left(1 - \frac{B}{N_t}\right) \cdot g_{i,j} g_{i,j}^\top + \frac{1}{B N} \cdot \left(1 - \frac{B}{N}\right) \sum_{j' \neq j} g_{i,j'} g_{i,j'}^\top. \quad (8)$$

B GNQ AS AN EXPLANATION FOR MODINV SUCCESS

We identified two classes of interest from the Database of Faces dataset: the class with the lowest GNQ (class 28) and the class with the highest GNQ (class 6). As shown in Fig. 9, the left image depicts poor reconstruction for the lowest GNQ class, while the right image demonstrates successful recovery for the highest GNQ class, showing increased vulnerability. Importantly, we noticed that high-GNQ examples are more likely to be *memorized*, which is validated as the reconstructed image (Fig. 9 b right) corresponds to the example (not class) with the highest GNQ in the entire dataset (Fig. 9 b left).

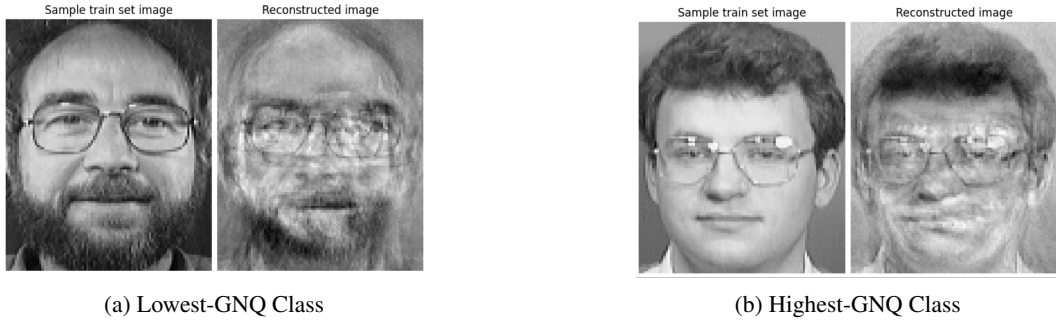


Figure 9: Reconstructed images for the lowest-GNQ class and the highest-GNQ class.